LA-UR -78-2607

CONF-780982--1

MASTER

TITLE: ULTRAVIOLET DAMAGE RESISTANCE OF LASER COATINGS

AUTHOR(S):

BRIAN E. NEWNAM

DENNIS H. GILL

SUBMITTED TO: Proceedings of
Tenth Symposium on Laser
Induced Damage Materials,
Boulder, CO Sept. 12-14, 1978

los alamos
scientific laboratory
of the University of California
LOS ALAMOS, NEW MEXICO 87545

EP

Form No. 836
St. No. 2629
1/75

UNITED STATES
ENERGY RESEARCH AND
DEVELOPMENT ADMINISTRATION
CONTRACT W-7405-ENG. 36

ULTRAVIOLET DAMAGE RESISTANCE OF LASER COATINGS*

Brian E. Newnam and Dennis H. Gill
Los Alamos Scientific Laboratory
Los Alamos, New Mexico 87545

The damage resistance of several thin-film materials used in ultraviolet laser optics was measured at 266 nm and 355 nm. The coatings included single, quarter-wave (QW) layers of NaF, LaF_3, MgF_2, ThO_2, Al_2O_3, HfO_2, ZrO_2, Y_2O_3 and SiO_2, plus multilayer reflectors composed of some of these materials. The substrates were uv-grade fused silica. Single-shot thresholds were obtained with 22 ns and 27 ns (FWHM) pulses at 266 and 355 nm, respectively. One of the samples had previously been tested using 20-ps pulses, providing a pulsewidth comparison.

At 266 nm the coating with the highest damage threshold was a QW layer of NaF at 10.8 J/cm^2 (450 MW/cm^2), whereas for a maximum reflector of Al_2O_3/NaF the value was 3.6 J/cm^2 (154 MW/cm^2), and the threshold of the maximum reflector was 12.2 J/cm^2 (470 MW/cm^2).

The results were analyzed to determine correlations with standing-wave electric fields and linear and two-photon absorption. Scaling relationships for wavelength, refractive index and atomic density, and pulsewidth were found.

Key words: damage thresholds; electric fields; laser damage; nanosecond pulses; pulsewidth dependence; standing waves; thin-film coatings; two-photon absorption; ultraviolet wavelength scaling.

1. Introduction

The recent growth in popularity of rare gas-halogen lasers has pointed up the lack of damage threshold data in the ultraviolet. This paper examines a variety of coating materials useful for uv laser optics. Single QW layers and multilayer total reflectors were irradiated at 266 nm (22 ns) and 355 nm (27 ns). Materials evaluated at both 355 nm and 266 nm were NaF, ThO_2, Al_2O_3 and ZrO_2. In addition, LaF , MgF_2, HfO_2, Y_2O_3 and SiO_2 were tested at 266 nm. Total reflectors of Al_2O_3/NaF and ThO_2/SiO_2 were tested at both wavelengths, and reflectors of ThO_2/MgF_2 and PbF_2/cryolite were tested at 266 nm. The film and substrate characteristics are listed in table 1. All coatings were deposited by use of an electron gun, except those by rf-sputtering as noted.

Table 1. Coating and substrate characteristics.

Coating Material	Substrate	Substrate Roughness Å rms	Substrate Deposition Temperature °C	Coating Index of Refraction 266 nm	355 nm	Coating Absorption Edge[a] nm
NaF	Suprasil 2	12	30	1.34	1.33	> 130
SiO_2 (sputtered)	Suprasil 2	12	165	1.52	1.51	> 160
MgF_2	Suprasil 2	12	30	1.39	1.38	> 115
LaF_3	Suprasil 2	12	30	1.61	1.60	> 135
ThO_2	Dynasil 1000	20	200	2.0	1.95	250
Al_2O_3	Suprasil 2	12	30	1.67	1.65	> 140
ZrO_2	Optosil 1	20	200	2.17	1.95	225
ZrO_2 (sputtered)	Suprasil 2	12	175	2.4	2.27	260
HfO_2	Ultrasil	20	250	2.15	2.08	220
Y_2O_3	Suprasil 2	12	200	2.0	1.79	215
Al_2O_3/NaF	Suprasil 2	12	30			
ThO_2/SiO_2	Dynasil 1000	20	200			
ThO_2/Mg	Dynasil 100	20	200			
PbF_2/Cryolite	Suprasil 2	12	30	2.17/1.37		230

[a] Film absorption edge defined where measured absorption was 10%. Values preceded by > are for bulk materials [1][1]; negligible absorption was measured for these coatings down to 200 nm.

* Work performed under the auspices of the U. S. Department of Energy.

1. Figures in brackets indicate the literature references at the end of this paper.

Most of the samples were on identical substrates of Suprasil 2 with approximately a 12 Å rms surface roughness. A few samples were on other types of uv-grade fused silica and had an approximate surface roughness of 20 Å rms. Spectrophotometric traces for the single QW layers are shown in figure 1. Note that some of the layers were not exactly $\lambda/4$ thick at 266 nm. The actual wavelength at which each coating was $\lambda/4$ thick is tabulated in tables 2 and 4.

The NaF single-layer samples were fogged in appearance. This was probably due to the high relative humidity in the coating company's plant (reported to be about 65%). However, Al_2O_3/NaF reflectors were not fogged, probably because the outer layer of Al_2O_3 protected the NaF. The gradual decline in transmission at shorter wavelengths for NaF (fig. 1) was due to scattering losses from the fog. Special note is also made of the short-wavelength transmission of the ThO_2 which did not extend to the expected absorption edge.

2. Experimental procedure

The experimental arrangement is shown in figure 2. A Nd:YAG laser was Q-switched using Bis (4-dimethylamino-dithiobenzil) nickel dye and 3 etalons inside the cavity. The combination of slow-relaxation-type dye and etalons produced a 35 ns pulse at 1064 nm. This beam was then frequency doubled and subsequently tripled or quadrupled. The 266 nm pulsewidth was nominally 22 ns and the 355 ns pulsewidth was nominally 27 ns. Two dispersive prisms were used to separate out the desired wavelength. Beam pickoffs reflected energy into a fast photodiode (ITT F4014) and a Laser Precision Energy Meter. The photodiode signal was sent to a Tektronix R7912 Transient Digitizer. Another beam pickoff was focused by a 500 mm fl lens, identical to that in the main beam path, onto a Reticon linear diode array, as shown in figure 2, or onto an aperture in front of another Laser Precision Energy Meter, as shown in figure 3. The Reticon array was used at 355 nm to determine focal spot size; it could not be used at 266 nm due to fluorescence of the array window.

The arrangement shown in figure 3 was used at both wavelengths to determine the energy dendity on the sample. The two apertures were 70 um diameter. Aperture 1 and Energy Meter 1 were located at the sample position, which was 450 mm from the 500 mm fl lens. After the calibration, these were removed and the samples placed at position 2 for the tests. Aperture 2 and Energy Meter 2 remained in position for the entire test. By determining the ratio of the transmitted energy in the two paths, path 2 could be used during the test to establish the energy density at the sample. Since the beam spot size was w = .5 mm radius at $1/e^2$ intensity, the beam profile was not completely flat across the aperture. A small correction factor (6.3%) was used to calculate the peak energy density.

Energies from the energy meters, time profiles from the R7912 and (at 355 nm) the spatial profile from the diode array were fed to an on-line computer and data acquisition system for immediate analysis [2]. The calculated energy density and power density were printed out after each shot for use in plotting the data or a scatter-plot as the test proceeded.

Each sample was irradiated with an average of about 40 shots. Each site was irradiated only once. Damage was determined by visual observation of the irradiated site through a 40X stereo microscope. Two types of illumination were used. A bright white light source illuminated the entire sample. A He-Ne laser illuminated only the actual irradiated zone. The laser-induced scattering of both light sources was used to determine the occurrence of damage.

3. Results

Table 2 lists the damage thresholds of the various single QW layer materials tested at 266 nm. The ranges quoted in the damage threshold columns are from the lowest values that did cause damage to the highest values that did not cause damage [3]. For each laser shot the computer integrated the photodiode signal and calculated an effective pulsewidth which was then used to calculate the peak power density. Thus the apparent pulsewidth one obtains by dividing energy density by power density is not a constant. The previously quoted pulsewidths of 22 ns for 266 nm and 27 ns for 355 nm are average values for all of the tests.

The peak internal eluctric field was calculated using a LASL code that computes the E-field distribution within a dielectric stack. The actual thicknesses of each layer were taken into account. The various layers were not exactly a quarter wave at 266 nm, as shown in table 2. Figure 4 shows the relative E-field-squared distribution within two materials, one whose index of refraction is less than the substrate and one whose index is greater than the substrate. The peak E-fields are substantially different for the two cases. Also shown in figure 4 is the effect of testing at 355 nm a coating that is QW thick at 266 nm.

The low index material with the highest damage threshold was NaF, in spite of its fogged appearance. The high index material with the highest damage threshold was LaF_3.

Table 2. Comparison of materials at 266 nm

Material	Thickness /4 at (nm)	Damage Threshold Energy Density J/cm^2	Power Density MW/cm^2	Peak Internal E-Field MV/cm
NaF	266	10.8 ± 1.7	450 ± 70	.37 ± .03
SiO_2 (sputtered)	532	9.4 ± 0.3	410 ± 10	.32 ± .01
MgF_2	266	6.8 ± 0.7	310 ± 30	.30 ± .02
LaF_3	250	6.7 ± 0.6	280 ± 30	.26 ± .01
ThO_2	290	2.8 ± 0.4	122 ± 17	.16 ± .01
Al_2O_3	266	2.6 ± 0.2	106 ± 10	.16 ± .01
ZrO_2	300	1.5 ± 0.1	67 ± 4	.11 ± .01
ZrO_2 (sputtered)	505	1.5 ± 0.1	66 ± 4	.13 ± .01
HfO_2	278	1.3 ± 0.2	68 ± 10	.11 ± .01
Y_2O_3	374	0.6 ± 0.2	31 ± 10	.08 ± .01
SiO_2 (Suprasil 2) (Front surface)	---	8.0 ± 0.3	350 ± 10	.29 ± .01

Table 3. Comparison of total reflectors at 266 nm.

Material	Damage Threshold Energy Density J/cm^2	Power Density MW/cm^2	Peak Internal E-Field MV/cm
Al_2O_3/NaF	3.6 ± .4	154 ± 17	.29 ± .02
ThO_2/SiO_2	1.3 ± .1	71 ± [illegible]	.16 ± .01
ThO_2/MgF_2	1.1 ± .3	55 ± 15	.14 ± .02
PbF_2/Cryolite	.5 ± .1	19 ± 4	.11 ± .01

Table 3 lists the four reflectors tested at 266 nm. The Al_2O_3/NaF reflector was the best by a considerable margin. The threshold of the PbF_2/Cryolite reflector was quite low.

The single layer materials tested at 355 nm are listed in table 4. It should be emphasized that these are the same, identical samples as those tested at 266 nm. At 38 J/cm^2 (1.39 GW/cm^2) we were unable to damage the NaF thin film. There were only small differences between the other three samples.

The two reflectors tested at 355 nm are listed in table 5. Again, the Al_2O_3/NaF was best by more than a factor of 2. The reflectors tested at 355 nm were not the same as those tested at 266, but rather were maximum reflectors at 355 nm made by the same company on the same day as the maximum reflectors at 266 nm.

All of the materials and reflectors that were tested at both wavelengths are brought together in table 6 for easier comparison. This data is then plotted in figure 5 in terms of energy density and in figure 6 in terms of electric field. Figure 7 is a plot of the data obtained previously [3] on some of the same materials at 1064, 532 and 355 nm. Pulsewidths for this data were 30 ps, 20 ps and 17 ps, respectively. Spot sizes were similar to the present data. The higher damage thresholds at 532 nm compared to those at 1064 nm were observed to be in accordance with the frequency dependence of the electron avalanche mechanism.

Table 4. Comparison of materials at 355 nm.

Material	Thickness λ/4 at (nm)	Damage Threshold Energy Density J/cm^2	Power Density MW/cm^2	Peak Internal E-Field MV/cm
NaF	266	> 38	> 1390	> .65
ThO_2	290	9.1 ± .2	340 ± 10	.27 ± .01
ZrO_2	300	7.1 ± .2	250 ± 10	.23 ± .01
Al_2O_3	266	5.9 ± .5	210 ± 20	.22 ± .01

Table 5. Comparison of total reflectors at 355 nm.

Material	Damage Threshold		
	Energy Density	Power Density	Peak Internal E-Field
	J/cm^2	MW/cm^2	MV/cm
Al_2O_3/NaF	12.2 ± .9	470 ± 40	.51 ± .02
ThO_2/SiO_2	4.9 ± .1	180 ± 10	.27 ± .01

Table 6. Spectral dependence of damage thresholds.

Material	Damage Thresholds			
	Energy Density (J/cm^2)		Peak E-Field (MV/cm)	
	266 nm	355 nm	266 nm	355 nm
NaF	10.8 ± 1.7	> 38	.37 ± .03	> .65
Al_2O_3	2.6 ± 0.2	5.9 ± 0.5	.16 ± .01	.22 ± .01
Al_2O_3/NaF Reflector	3.6 ± 0.4	12.2 ± 0.9	.29 ± .02	.51 ± .02
ThO_2	2.8 ± 0.4	9.1 ± 0.2	.16 ± .01	.27 ± .01
ThO_2/SiO_2 Reflector	1.3 ± 0.1	4.9 ± 0.1	.16 ± .01	.27 ± .01
ZrO_2	1.5 ± 0.1	7.1 ± 0.2	.11 ± .01	.23 ± .01

4. Discussion

4.1. Electric-field correlations

Several experimental studies with short laser pulses (30 ps-10ns) have determined that coating damage occurs first at the locations of internal electric field maxima [4,5]. Accordingly, the threshold electric fields listed in tables 2-6 have also been computed at the standing wave (SW) maxima, however, at our relatively longer (20-30 ns) pulses, a complete analysis should include thermal conduction during the pulse which reduces temperature extremes at SW peaks. This is more applicable for coatings which damage by absorption than by avalanche breakdown.

An exact correlation of peak electric fields for 22 ns pulses at 266 nm is found with ThO_2 coatings. A breakdown field of 0.16 MV/cm was measured for ThO_2 both as a single-layer and in the reflector configuration of ThO_2/SiO_2 (table 6). (Damage occurs first in the high-index layer of the reflector).

A correlation of peak fields was <u>not</u> observed in Al_2O_3 coatings, however. The respective threshold fields in single-layer and reflector configurations (Al_2O_3/NaF) were 0.16 and 0.29 MV/cm. There are two apparent explanations for the difference. One is that the Al_2O_3 single-layer had greater absorption or was weaker, a fact which would be difficult to specifically measure. The second possibility is that the material adjacent to the Al_2O_3 was influential.

To discuss the latter, we first note that the peak fields in both coating configurations occurred at the interfaces with adjacent material, the fused silica substrate for the QW case and the first NaF layer in the reflector. If absorption is the damage mechanism, then thermal conduction away from the interfaces during the 22 ns pulse must be considered. Since the thermal diffusivity of NaF at 0.070 cm^2/sec (bulk, 300°K) is an order of magnitude greater than that of fused silica (0.0083 cm^2/sec) [6], conduction losses at the interfaces could well have been significantly different. Additionally, coating damage could have resulted from heating of inclusions in the polished surface layer of the silica substrate. Further experiments would be required to determine which is the correct explanation.

4.2. Spectral Dependence

4.2.1. Linear and two-photon absorption

The decline in damage resistance at 266 nm when compared to that at 355 nm (shown in figures 5 and 6) was anticipated. Linear absorption increases rapidly as the absorption band edge is approached. Besides linear absorption, multiphoton absorption also becomes a potential damage mechanism. As can be deduced from the values of absorption edge listed in table 1, two-photon absorption (TPA) is energetically possible for all of the coating materials for 266 nm irradiation. At 355 nm, TPA is also possible for ThO_2, ZrO_2, HfO_2, Y_2O_3 and PbF_2, but 3 photons are required for resonant absorption in the remaining coatings listed.

In a previous study with picosecond pulses at 355 nm, Newnam and Gill [3] suggested that TPA was a plausible damage mechanism for ZrO_2, HfO_2, and SiO_2. This possibility could not be confirmed because TPA coefficients (β) were not known, nor were accurate linear absorption coefficients (α) measured by calorimetric techniques available. Derivation of α from spectrophotometric curves is subject to error when coating inhomogeneity (variation of refractive index with thickness) and scattering losses are not well quantified. Unfortunately, a similar deficiency in film characterization existed in this study. However, recent measurements of TPA coefficients of laser crystals and windows at 266 and 355 nm reported by Liu, et al. [7], allow estimation of the relative role of TPA for a few of the coatings in this study.

In absorption processes, the power absorbed per unit volume, dI/dz, is the quantity of interest. For both first and second-order absorption,

$$\frac{dI}{dz} = -\alpha I - \beta I^2 \quad . \tag{1}$$

When the plane-wave expressions for I ($= \frac{1}{2} \quad u/\varepsilon|E|^2$) and I_o (incident) are substituted, we obtain

$$\frac{dI}{dz} = -nI_o \left(\frac{E(z)}{E_o^+}\right)^2 (\alpha + \gamma), \tag{2}$$

where

$$\gamma = \beta n I_o \left(\frac{E(z)}{E_o^+}\right)^2, \tag{3}$$

and $|E(z)/E_o^+|^2$ is the standing-wave distribution normalized to the incident field. To heat a material to its melting point (a well-defined damage threshold), the minimum <u>total</u> absorption coefficient α_T (cm^{-1}) is given by

$$\alpha_T = \frac{\rho c_p}{n} (T_{mp} - 300°K) \left|\frac{E(z)}{E_o^+}\right|^{-2}_{peak}, \tag{4}$$

where ρ is density, c_p is specific heat, and E_o is the incident energy density threshold.

From calculations of α_T and γ using experimentally measured damage thresholds, it is possible to determine the relative role of 1- and 2-photon absorption in the damage process, ignoring other possible competing mechanisms. The reported values of β (cm/MW) at 266 and 355 nm for Al_2O_3 are 2.7×10^{-4} and $< 1.6 \times 10^{-5}$, and for fused silica are $\leq 4.5 \times 10^{-5}$ and $< 1.3 \times 10^{-6}$, respectively [7]. Values for other coating materials tested in this study are not available except for ZrO_2 for which β at 694 nm was reported to be 2.4×10^{-3} cm/MW [8]. Corresponding values at uv wavelengths would, of coutse, be much larger. Computed values of α_T and γ are shown in table 7. For purposes of comparison, typical values of α for thick commercially deposited coatings are presented in table 8.

The primary observation is that for nanosecond pulses 2-photon absorption is not an important damage mechanism for these three materials. Only for picosecond-pulse irradiation of ZrO_2 is it significant. Secondly, nanosecond-pulse damage to ZrO_2 coatings at 266 nm occurred via linear absorption. The value of α_T to cause melting is within the value listed in table 8. At 355 nm, the computed α_T of 900 cm^{-1} for ZrO_2 exceeds that in table 8 (210 cm^{-1}) by a considerable amount. Possibly, absorbing coating defects were damaged at a lower laser intensity.

Table 7. Total and two-photon absorption contributions to uv laser coatings damage.

Coating Material	266 nm		355 nm	
	$\alpha_T(cm^{-1})$	$\gamma(cm^{-1})$	$\alpha_T(cm^{-1})$	$\gamma(cm^{-1})$
Pulsewidth	(22 ns)		(27 ns)	
ZrO_2 (E-gun)	3400	> 1	900	> 1
ZrO_2 (sputtered)	2900	> 1	--	--
Al_2O_3	2300	0.03	1000	0.001
Al_2O_3 (in reflector)	700	0.10	200	0.002
SiO_2 (sputtered)	250	0.02	--	--
SiO_2 (substrate)	350	0.02	--	--
			(17 ps)	
SrO_2 (E-gun)	--	--	2800	> 300
SiO_2 (E-gun)	--	--	1000	< 0.2

Table 8. Typical absorption coefficients for thick uv coatings deposited by electron-gun [9]

$\alpha(cm^{-1})$

Coating Material	250 nm	350 nm
ZrO_2	6000	210
HfO_2	950	270
Al_2O_3	190	150
LaF_3	850	430
PbF_2	900	100

Computed values of α_T for Al_2O_3 are much in excess of typical values. As these coatings were deposited at ambient temperature and with no reactive exygen atmosphere, the oxidation of the Al probably was not complete, resulting in high absorption.

Finally, linear absorption at 266 nm was probably the operative damage mechanism for the other oxides, Y_2O_3, HfO_2 and ThO_2, although the available evidence is not conclusive.

4.2.2. Wavelength scaling

The spectral dependence of laser damage in figure 6 suggests an interesting relationship between the electric field thresholds at 355 and 266 nm. For the coating materials, NaF, Al_2O_3, ThO_2 and ZrO_2, which were tested at both wavelengths, the ratio of the threshold fields is

$$\frac{E_t(355}{E_t(266)} = 1.73 \pm 0.23 \qquad (5)$$

This is surprisingly close to the ratio of the laser wavelengths squared, i.e. $(355/266)^2 = 1.78$!

It is probably permissable to use this wavelength-squared ratio to estimate the 355 nm thresholds of coating materials only tested at 266 nm (see Tables 1 and 4) since the wavelength range is narrow. However, the relationship $E_t \sim \lambda^2$ observed here is <u>not</u> expecced to be a general scaling law for laser damage at ultraviolet wavelengths. Such a dependence is not generally derivable from the theory of optical absorption in dielectrics. That theory predicts that the absorption coefficient at a frequency ν near the center frequency of an absorption band ν_0 is of the form

$$\alpha \sim \frac{\gamma^2\nu^2}{(\nu_0^2-\nu^2)+\gamma^2\nu^2}, \qquad (6)$$

where γ is a material constant acounting for the breadth of the absorption band [10]. The subject of a wavelength scaling law for uv laser damage merits further consideration.

4.3. Refractive-index and atomic density scaling

In a number of laser damage studies of thin film materials used in the visible and near ir regions, high-index coatings have been found to damage more easily than low-index coatings [11, 12, 13, 14, 15]. Bettis, et al, [14], have derived a first principles equation for the macroscopic breakdown electric field in terms of material parameters,

$$E_{th} = \frac{N}{n^2-1}\ \frac{q_e}{\varepsilon_0}\ X_{cr}\sqrt{10^{-5}} \qquad (7)$$

where N is atomic density (cm^{-3}), n is refractive index, q_e is electronic charge and X_{cr} is the critical separation required to free an optical electron from its atom. The threshold fields for a number of coating materials, when irradiated with 40-ns, 1.06 μm pulses, were shown to follow this relationship fairly well.[14].

The present coating thresholds for 266 nm have been plotted versus $N/(n^2-1)$ (the dominant term in eq. (7)) in figure 8. A straight line provides a reasonable fit to the data with certain exceptions. The threshold for NaF was considered low, due to fogging, MgF_2 is generally an inhomogeneous film with substantial H_2O content, and the single-layer Al_2O_3 had an anomalously low threshold, probably due to high absorption. A least-squares straight-line fit of the data in figure 8, ignoring the points for lossy films of NaF, MgF_2, and single-layer Al_2O_3, provides the equation

$$E_{th}(MV/cm \sim 0.54\ \frac{N}{n^2-1} \qquad (8)$$

Certain corrections could be applied to improve the observed correlation. First, the atomic density, N, should be multiplied by the coating packing density since coatings are not as dense as bulk crystals. For example, p = 0.72 for MgF_2 deposited at 30°C before exposure to the atmosphere [16]. Secondly, HfO_2 and ThO_2 coatings were deposited on slightly rougher substrates that the other films (∿ 20 Å rms as compared to ∿ 12 A rms). House, et al.[17], have demonstrated that increased substrate roughness decreases the damage threshold field as $E_{th} \sim \sigma^{-0.5}$, so the thresholds for HfO_2 and ThO_2 could be

adjusted upward about 25% for comparison purposes.

4.4. Pulsewidth dependence

A pulsewidth dependence of laser damage at 355 nm for a single-layer coating of ZrO_2 on Optosil 1 is shown in figure 9 in which the present measurements at 27 ns are compared to a previous measurement at ∿ 20 ps on the same sample. [3]. The laser spot-size radii were slightly different, 120 μm versus 150 μm, but this does not prevent a direct comparison. (For 30-ps pulses, no significant threshold dependence on spot-size was measured [3].) The observed $\tau^{1/6}$ dependence for energy density threshold is much more gradual than the 1/2-power dependence observed for the bulk and surfaces of many window materials [18].

In previous measurements at 694 nm over a pulsewidth range of 12 to 34 ns, a $\tau^{1/2}$ dependence was measured for a single half-wave coating of ZrO_2 only when the occurrence of a photometrically detectable spark was used as the criterion for damage [12]. Using the more sensitive technique of laser-induced scatter as the damage criterion, only a $\tau^{1/3}$ dependence was measured for the same sample. In another study at 694 nm at 20 ps and 23 ns, Bliss, et al. [19], measured the thresholds (J/cm^2) of ZrO_2/SiO_2 reflectors to increase as $\tau^{1/3}$ to $\tau^{1/2}$. In their tests, a spark was visible on most shots causing detectable damage.

From the above and other observations, one may conclude that the energy density damage threshold of coatings generally increases with pulsewidth at a rate less than or equal to $\tau^{1/2}$. For the ZrO_2 coating tested in this series at 355 nm, a much weaker dependence was measured.

5. Summary

The damage thresholds of a variety of single-layer coatings and multilayer reflectors were measured at 266 nm and 355 nm using 22- and 27-ns pulses, respectively. The coating materials included NaF, cryolite, MgF_2, SiO_2, LaF_3, Al_2O_3, ThO_2, HfO_2, Y_2O_3, ZrO_2 and PbF_2. The principal findings of this study were:

a. Reflectors comprised of Al_2O_3 and NaF layers had the highest thresholds (3.6 J/cm^2 at 266 nm and 12 J/cm^2 at 355 nm). In a fluorine-gas environment a LaF_3/NaF multilayer would be suggested.

b. The single-layer coating with the highest threshold was NaF (11 J/cm^2 or 0.37 MV/cm at 266 nm and 38 J/cm^2 or 0.65 MV/cm at 355 nm), although the coating was fogged by exposure to a humid atmosphere.

c. The electric-field thresholds at the SW maxima in a ThO_2 single layer and in a ThO_2/SiO_2 reflector were equal. A correlation of peak fields for similar Al_2O_3 coatings was not observed, presumably because the coatings had unequal linear absorption or because of the differing thermal diffusivities of the adjacent materials.

d. The electric field threshold (internal peak value) is related to the atomic density N and the refractive index in the form $N/(n^2-1)$. At 266 nm the relationship was $E_t \sim 0.54\ N/(n^2 01)$.

e. Two-photon absorption was not an important damage mechanism for 20-ns pulse damage at 266 and 355 nm for coatings of ZrO_2, Al_2O_3 and SiO_2. (For 20-ps pulses, however, TPA is substantial in ZrO_2 at 355 nm.) For the other coating materials, measurements of TPA coefficients are required before conclusions are possible.

f. Linear absorption was responsible for damage of ZrO_2 at 266 nm; failure at 355 nm may have occurred at sites of absorbing inclusions. Damage of HfO_2, ThO_2, Y_2O_3 and Al_2O_3 was probably caused by the same mechanisms, although the available evidence was insufficient.

g. A wavelength scaling relationship of $E_t(MV/cm) \sim \lambda^2$ was discovered for several coatings between 266 and 355 nm. Though not derivable from basic theory, it can be useful for estimating relative thresholds in this restricted spectral range.

h. Increased damage resistance at longer pulsewidths was measured at 355 nm for a ZrO_2 coating. From data points at 20 ps and 27 ns, a threshold relationship of $\mathcal{E}(J/cm^2) \sim \tau^{1/6}$ was apparent. This is a much more gradual pulsewidth dependence than $\tau^{1/2}$, which has been observed for uncontaminated laser window materials.

6. Acknowledgements

The authors gratefully acknowledge the technical assistance of John Meier in conducting the damage tests. The following persons and companies supplied thin-film coatings that were used in the tests and provided technical information about the coatings: Joe Latore, Lambda/Airtron; Verne Costich, Design Optics; Alex Shimkunas, Optical Coating Laboratory, Inc.; Jim Lavin, Laser Optics; Manfred Grindel, Continental Optical; John Hartmann, Battelle Pacific Northwest; and Phillip Baumeister, University of Rochester. The substrates were polished by Laser Optics.

7. References

[1]. Sparks, M., Sen, P.N., Flannery, M., and Loh, Jr., F., Theoretical Studies of High-Power Ultraviolet and Infrared Materials, Final Tech. Report, Contract DAHC15-73-C-0127, p. 225, March 31, 1978.

[2]. Kuckertz, T. H. and Gill, D. H., Proceedings of Eleventh Hawaii Int'l. Conf. on System Sciences, p. 162 (1978).

[3]. Newnam, B. E., and Gill, D. H., NBS Spec. Pub. 462, 292 (1976).

[4]. Apfel, J. H., Matteucci, J. S., Newman, B. E. and Gill, D. H., NBS Spec. Publ 462,301 (1976)

[5]. Newnam, B. E., "Laser Induced Damage Phenomena in Dielectric Films, Solids, and Inorganic Liquids," Ph.D. dissertation No. 73-09, 317, University Microfilm, Ann Arbor, Md.

[6]. Moses, A. J., Handbook of Electronic Materials, Vol. 1: Optical Materials Properties, (IFI/Plenum, New York, 1971), pp. 68,82.

[7]. Liu, P., Smith, W. L., Lotem, H., Bechtel, J. H., Bloembergen, N., and Adhav, R. S., NBS Spec. Pub. 509, 489 (1977).

[8]. Picard, R. H., Milam, D., Bradbury, R. A., and Fan, J. C. C., NBS Spec. Pub. 435, 272 (1976).

[9]. Costich, Berne R., Design Optics, private communication.

[10]. Seitz, F., The Modern Theory of Solids, (McGraw-Hill, New York, 1940), p. 634.

[11]. Turner, A. F., NBS Spec. Pub. 356, 119 (1971).

[12]. Newnam, B. D., and DeShazer, L. G., NBS Spec. Pub. 372,123 (1972).

[13]. Newnam, B. E., and Gill, D. H., NBS Spec. Pub. 435, 254 (1976).

[14]. Bettis, J. R., House, R. A., Guenther, A. H., and Austin, R., NBS Spec. Pub. 435, 289 (1976).

[15]. Smith, W. L., Milam, D., Weber, M. J., Guenther, A. H., Bettis, J. R., and House, R. A., NBS Spec. Pub. 509, 244 (1977).

[16]. Ritter, E., App. Opt. 15, 2318 (1976).

[17]. House, R. A., Bettis, J. R., Guenther, A. H., and Austin, R., NBS Spec. Pub. 435, 305 (1975).

[18]. Bettis, J. R., House, R. A., Guenther, A. H., NBS Spec. Pub. 462, 338 (1976).

[19]. Bliss, E. S., and Milam, D. NBS Spec. Pub. 372, 108 (1972).

8. Figure captions

Figure 1. Spectral transmittance for single QW coatings used in laser damage tests.

Figure 2. Experimental arrangement for performance of damage tests.

Figure 3. Experimental arrangement for calibration of axial energy density.

Figure 4. Distribution of standing-wave electric-field-squared in two single QW films, irradiated at 266 and 355 nm.

Figure 5. Spectral dependence of energy density threshold for damage of coating materials and reflectors. Pulsewidths were 22 ns and 27 ns for 266 nm and 355 nm, respectively.

Figure 6. Spectral dependence of electric field treshold for damage of coating materials and reflectors. Pulsewidths were same as for figure 5.

Figure 7. Spectral dependence of electric field treshold for damage of four coating materials. Pulsewidths were 30 ps, 20 ps, and 17 ps for 1064 nm, 532 nm, and 355 nm, respectively (from Ref. 3).

Figure 8. Electric field treshold versus $N/(n^2-1)$ for optical coatings irradiated at 266 nm.

Figure 9. Pulsewidth dependence of threshold energy density for single QW layer of ZrO_2 at 355 nm. Picosecond data from Ref. 3.

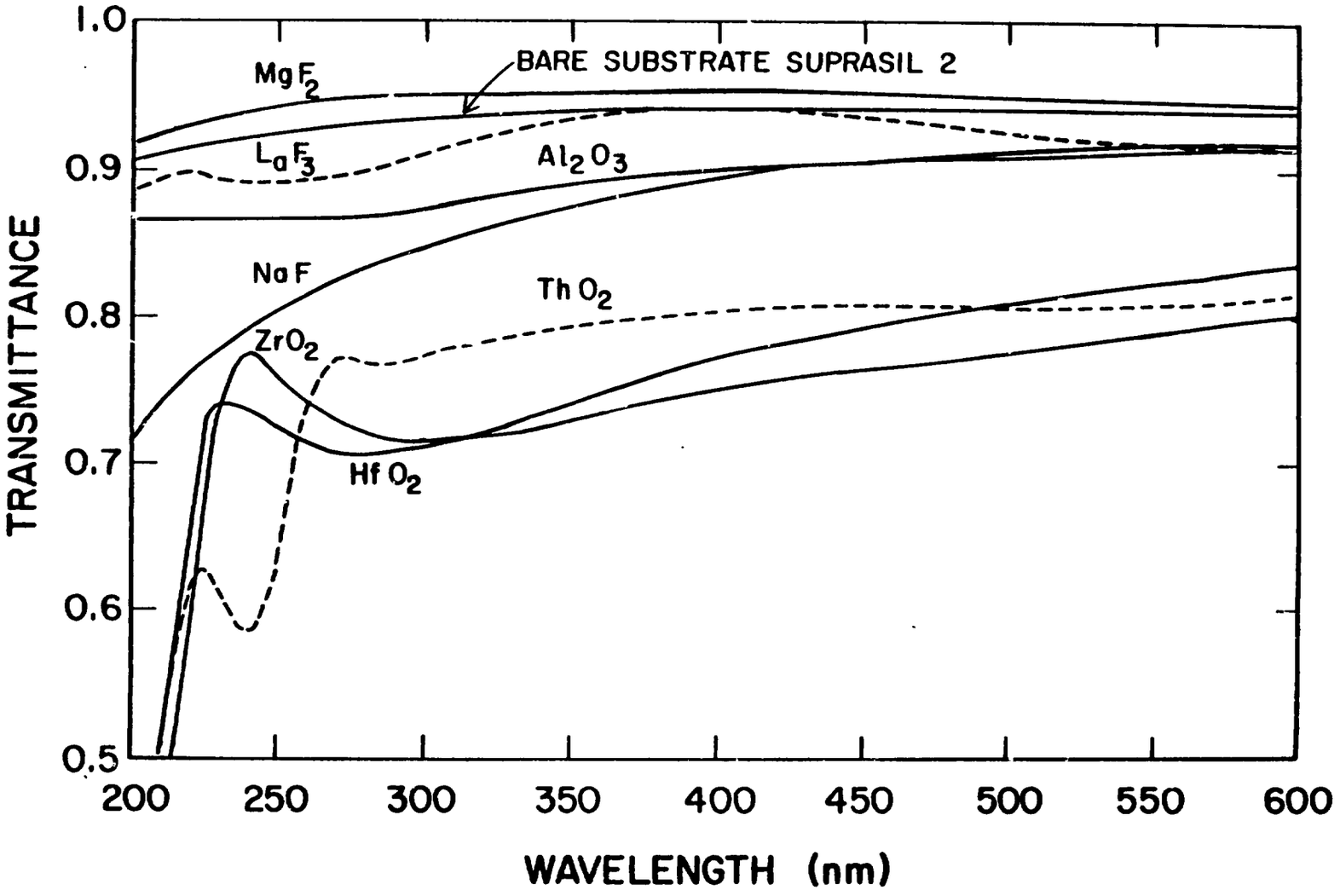
1.0
0.9
0.8
0.7
0.6
0.5
TRANSMITTANCE
200
250
300
350
400
450
500
550
600
WAVELENGTH (nm)
BARE SUBSTRATE SUPRASIL 2
MgF2
LaF3
Al2O3
NaF
ThO2
ZrO2
HfO2

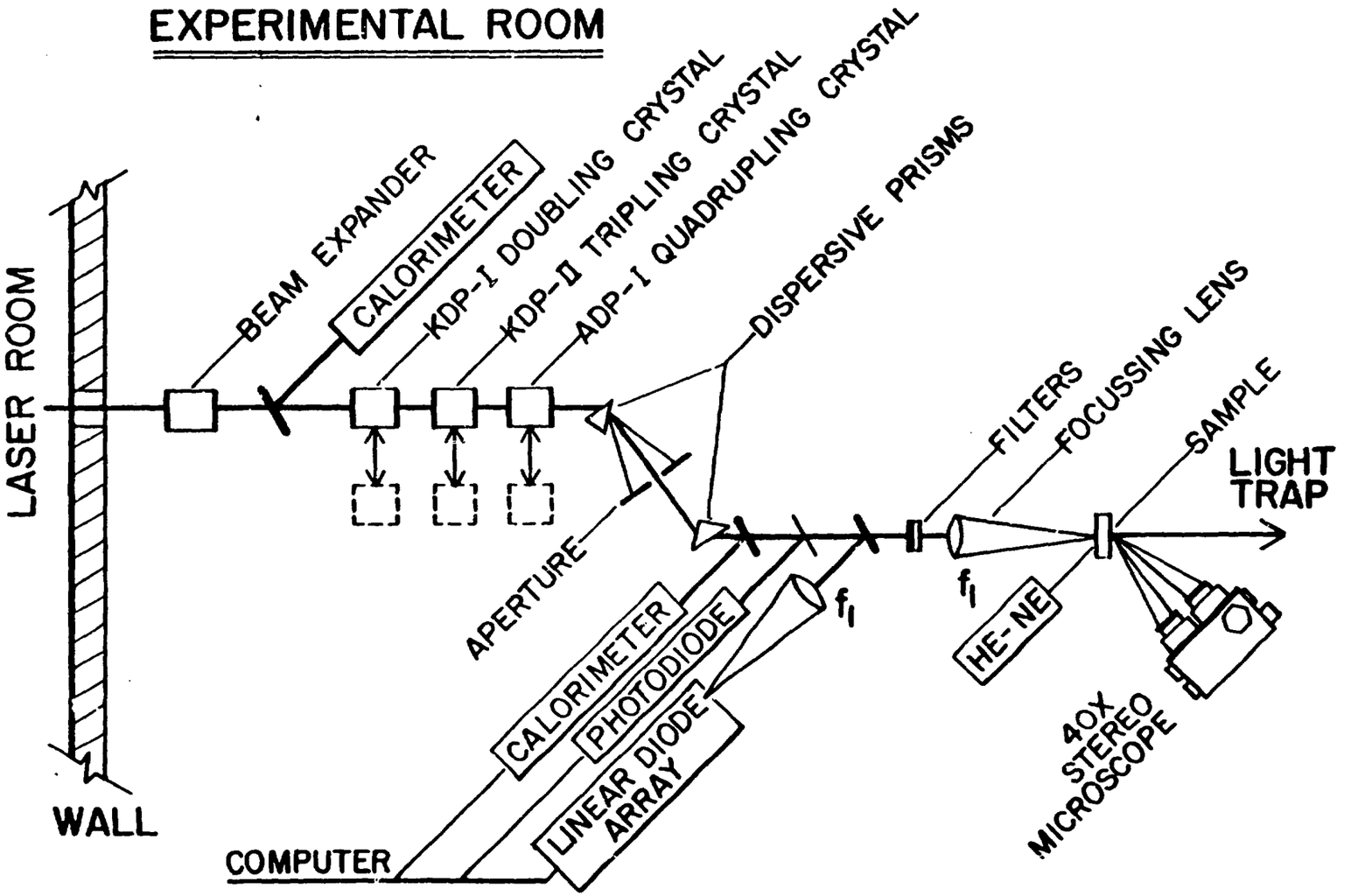
EXPERIMENTAL ROOM
LASER ROOM
WALL
BEAM EXPANDER
CALORIMETER
KDP-I DOUBLING CRYSTAL
KDP-II TRIPLING CRYSTAL
ADP-I QUADRUPLING CRYSTAL
DISPERSIVE PRISMS
APERTURE
CALORIMETER
PHOTODIODE
LINEAR DIODE ARRAY
COMPUTER
f_1
f_1
HE-NE
FILTERS
FOCUSSING LENS
SAMPLE
LIGHT TRAP
40X STEREO MICROSCOPE

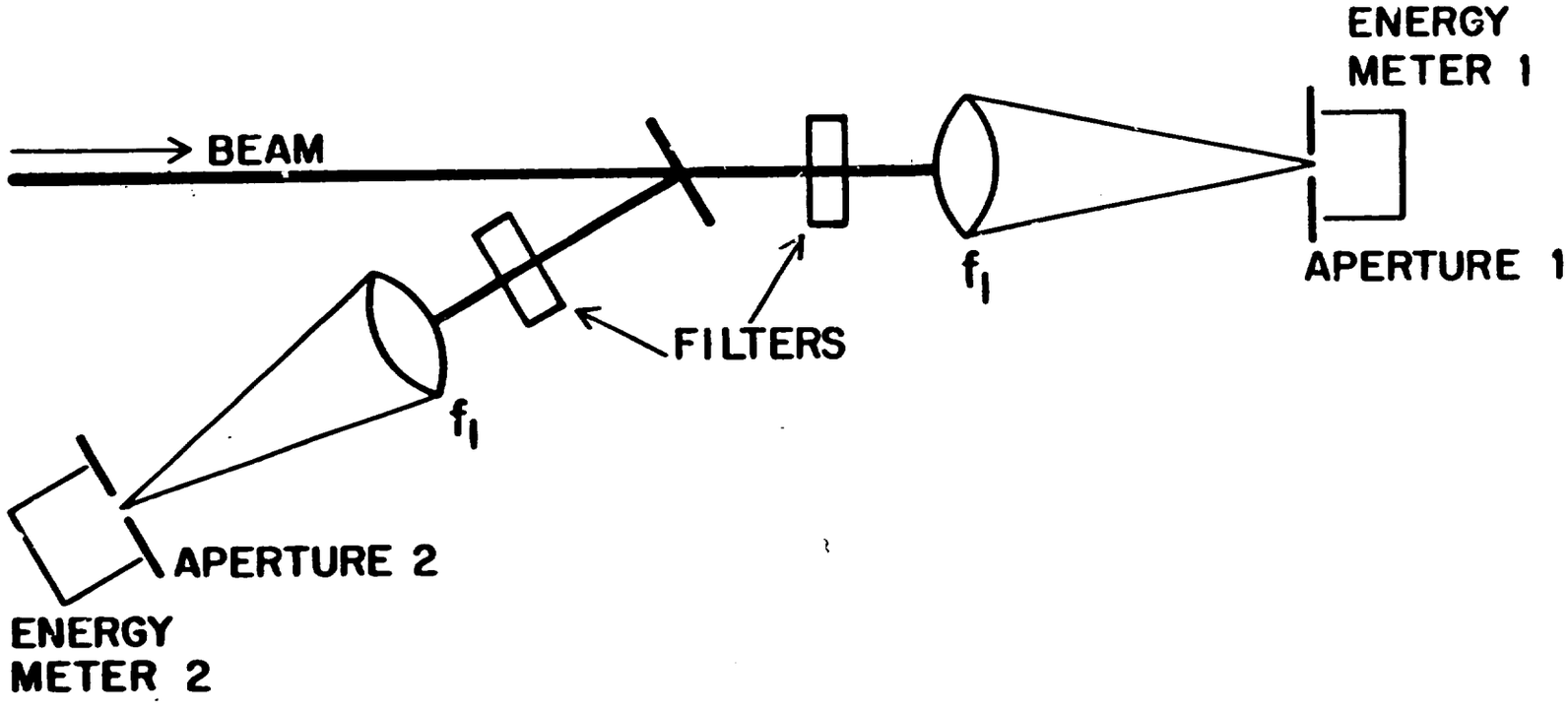
ENERGY
METER 1
BEAM
APERTURE 1
f_1
FILTERS
f_1
APERTURE 2
ENERGY
METER 2

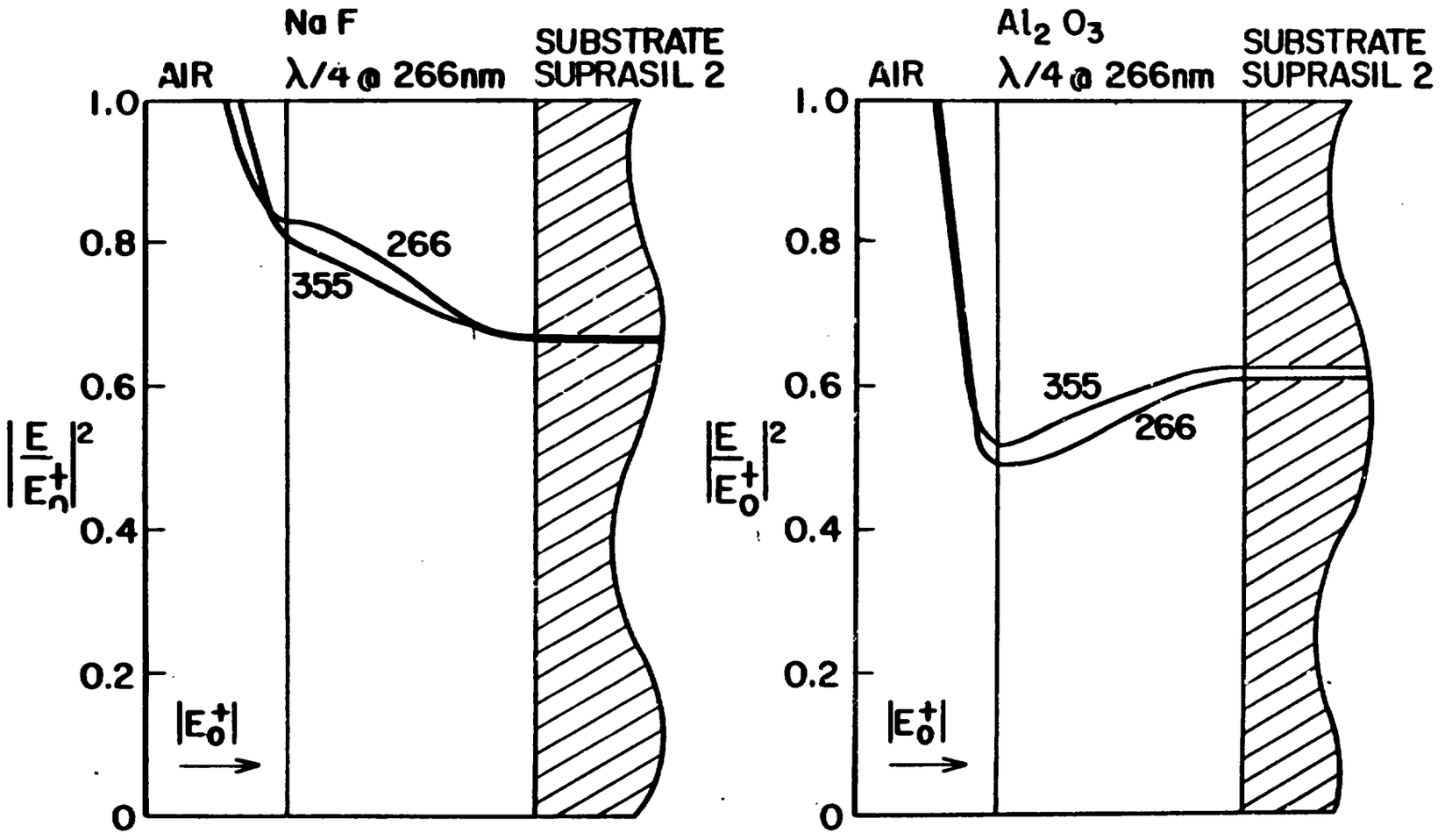
Na F
AIR
λ/4 @ 266nm
SUBSTRATE
SUPRASIL 2
1.0
0.8
0.6
0.4
0.2
0
266
355
$\left|\frac{E}{E_0^+}\right|^2$
$|E_0^+|$
Al_2O_3
AIR
λ/4 @ 266nm
SUBSTRATE
SUPRASIL 2
1.0
0.8
0.6
0.4
0.2
0
355
266
$\left|\frac{E}{E_0^+}\right|^2$
$|E_0^+|$

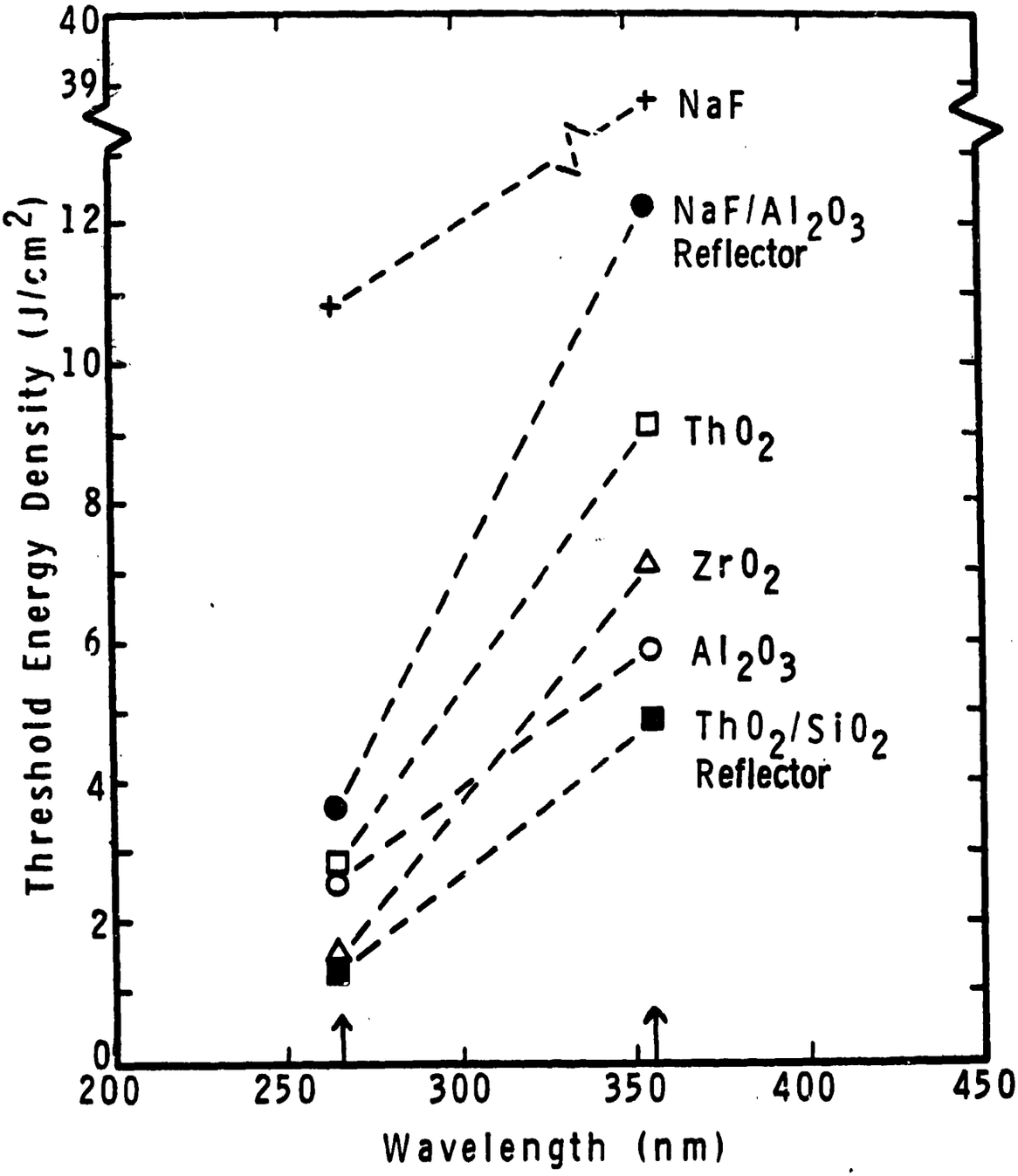
40
39
12
10
8
6
4
2
0
Threshold Energy Density (J/cm²)
NaF
NaF/Al₂O₃ Reflector
ThO₂
ZrO₂
Al₂O₃
ThO₂/SiO₂ Reflector
200
250
300
350
400
450
Wavelength (nm)

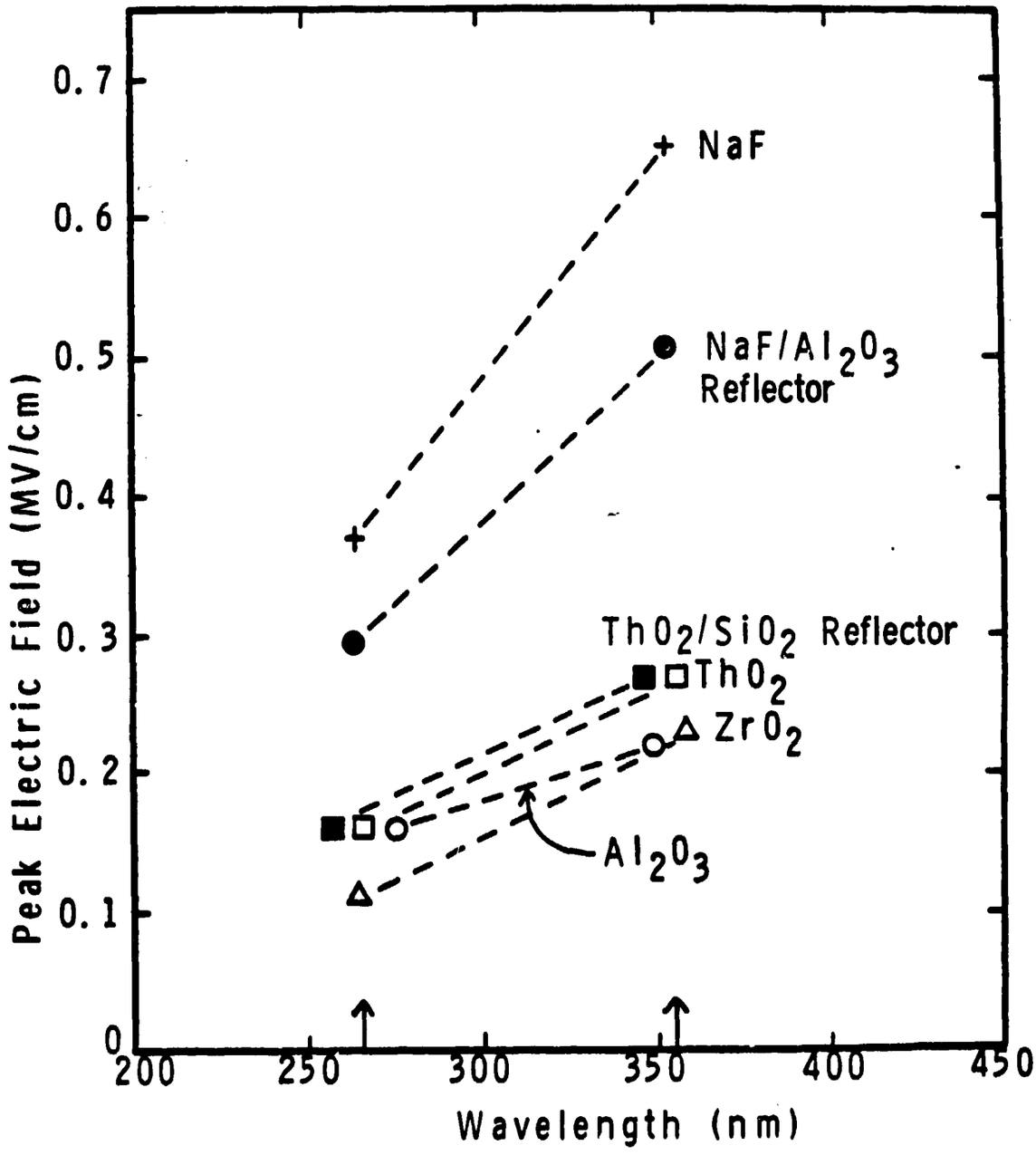
0.7
0.6
0.5
0.4
0.3
0.2
0.1
0
Peak Electric Field (MV/cm)
NaF
NaF/Al2O3
Reflector
ThO2/SiO2 Reflector
ThO2
ZrO2
Al2O3
200
250
300
350
400
450
Wavelength (nm)

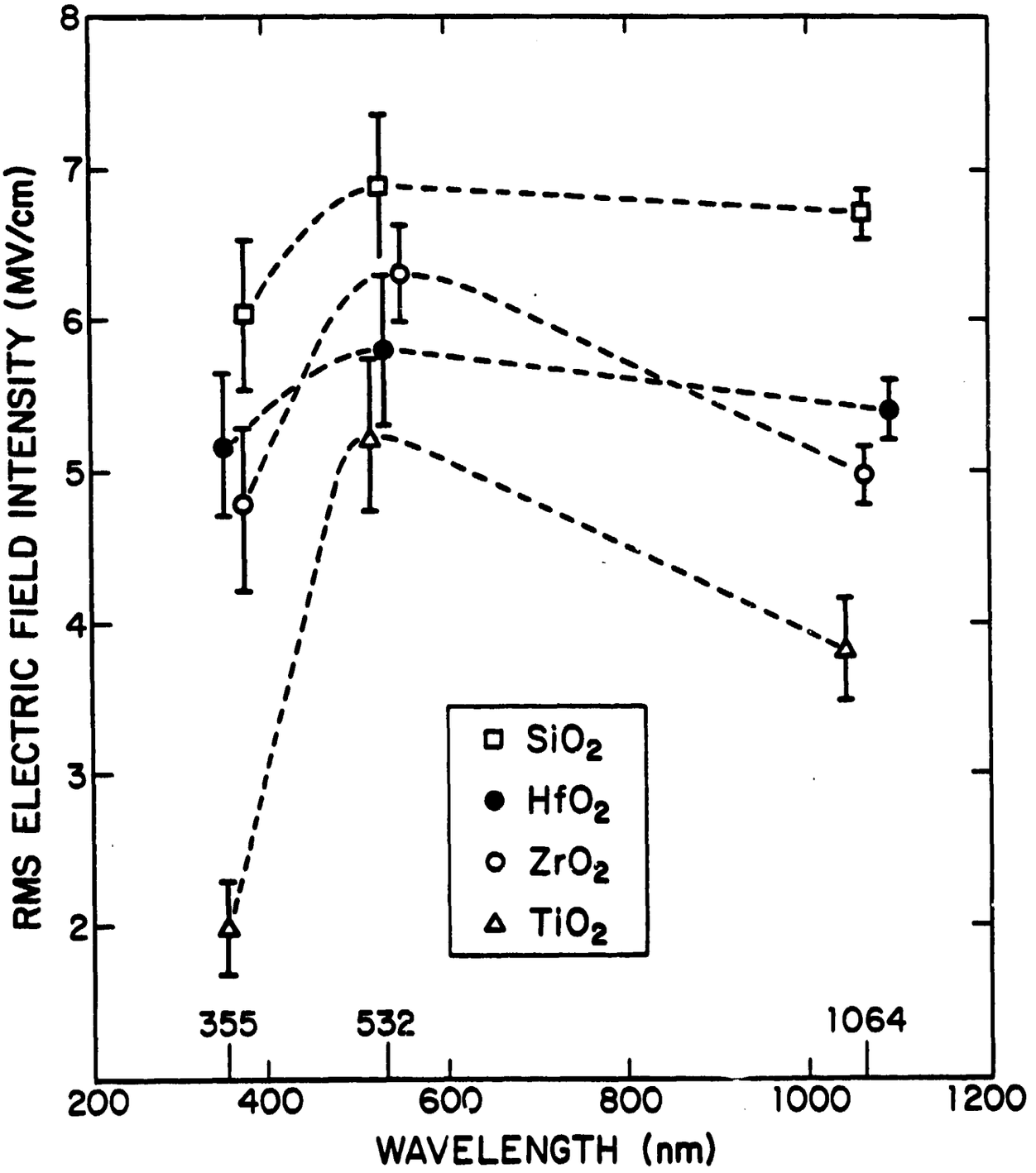
RMS ELECTRIC FIELD INTENSITY (MV/cm)
WAVELENGTH (nm)
8
7
6
5
4
3
2
200
400
600
800
1000
1200
355
532
1064
SiO2
HfO2
ZrO2
TiO2

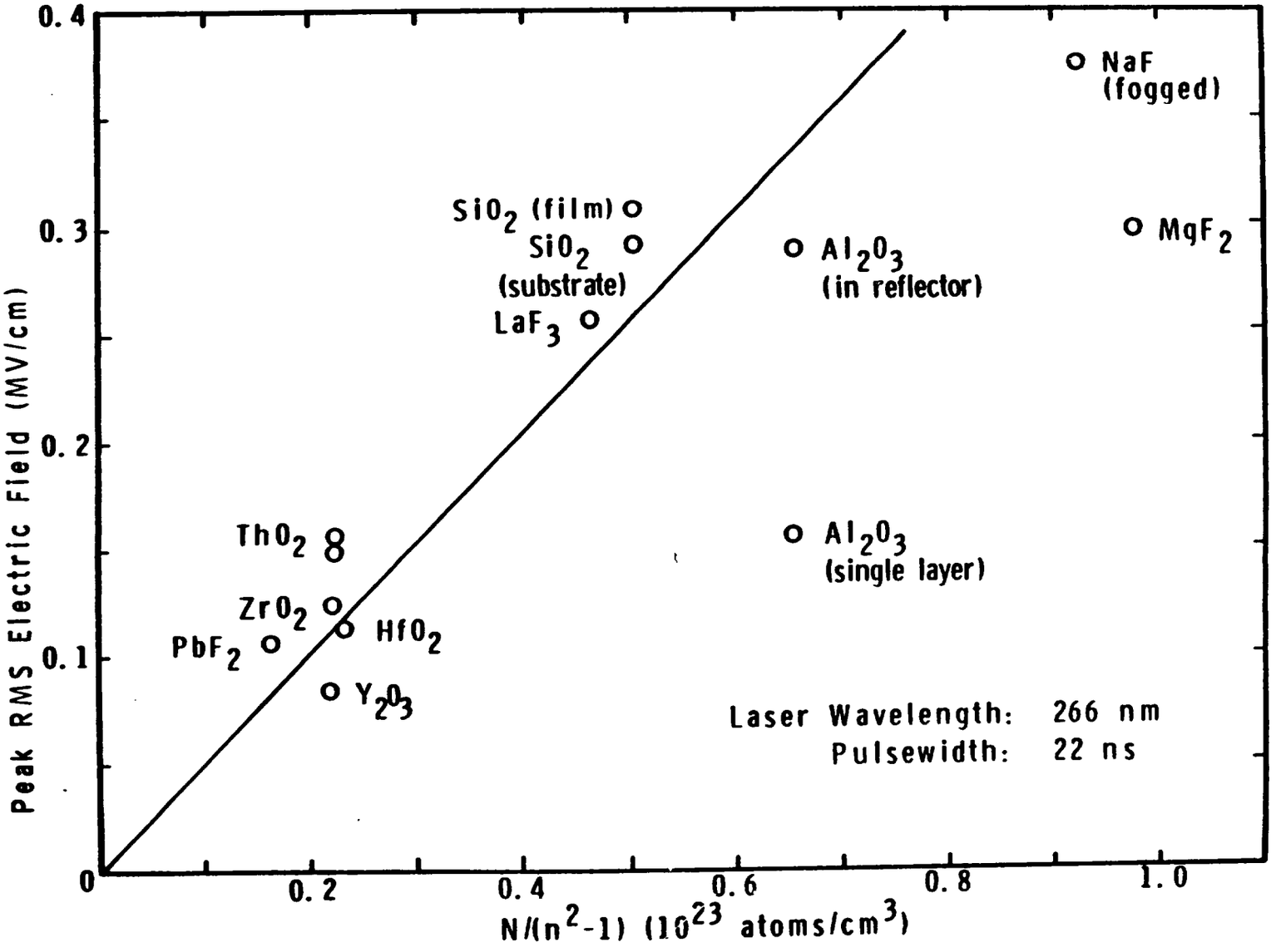
0.4
0.3
0.2
0.1
0
0.2
0.4
0.6
0.8
1.0
Peak RMS Electric Field (MV/cm)
N/(n²-1) (10²³ atoms/cm³)
NaF (fogged)
MgF₂
SiO₂ (film)
SiO₂ (substrate)
LaF₃
Al₂O₃ (in reflector)
Al₂O₃ (single layer)
ThO₂
ZrO₂
HfO₂
PbF₂
Y₂O₃
Laser Wavelength: 266 nm
Pulsewidth: 22 ns

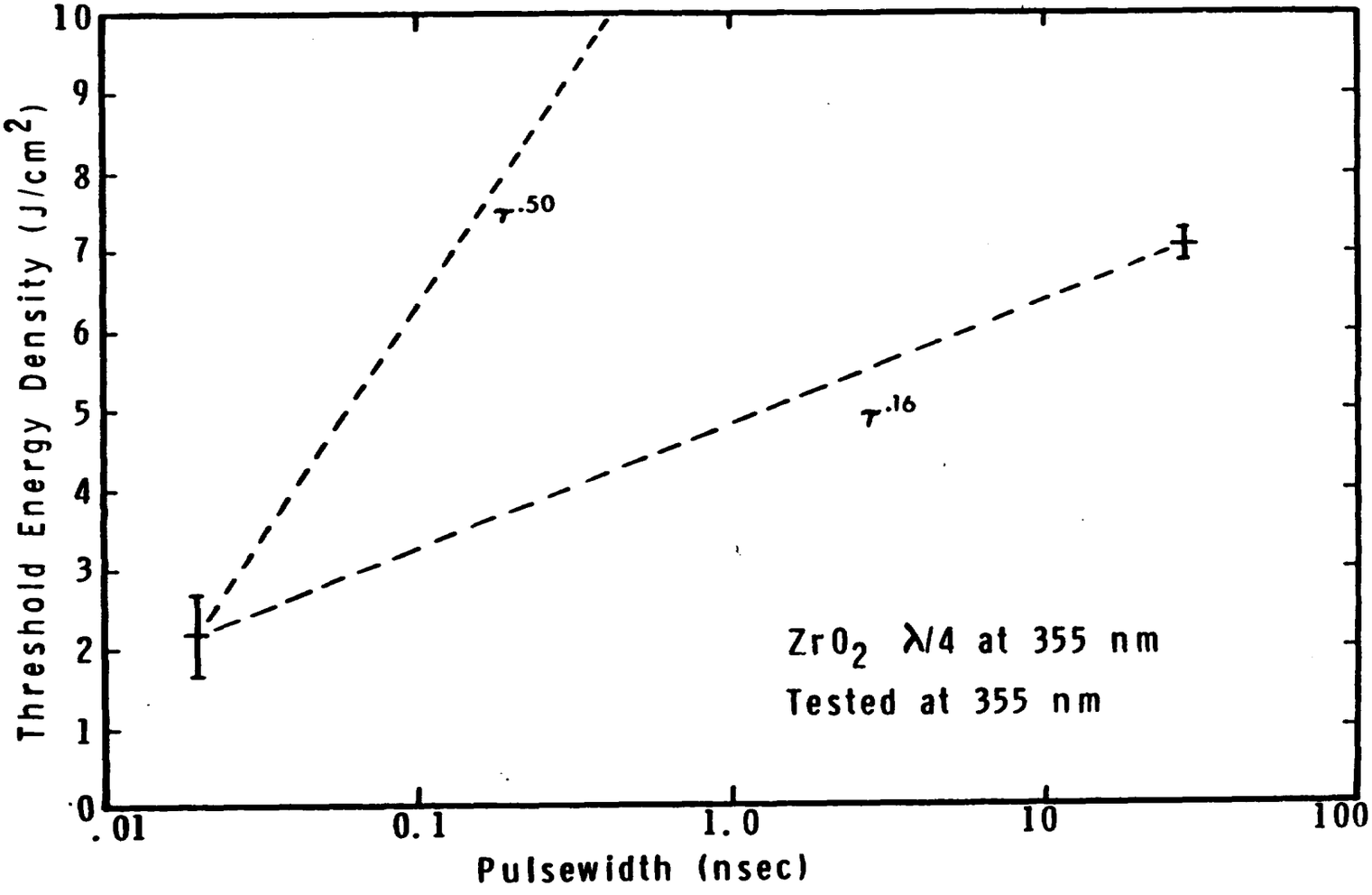
Threshold Energy Density (J/cm²)
10
9
8
7
6
5
4
3
2
1
0
τ^-.50
τ^-.16
ZrO2 λ/4 at 355 nm
Tested at 355 nm
.01
0.1
1.0
10
100
Pulsewidth (nsec)